Effects of the Horizontal Scales of the Cloud-Resolving Model on Tropical Cyclones in the Superparameterized Community Atmosphere Model

Kuan-Ting Kuo[1], Chien-Ming Wu[1], and Wei-Ting Chen[1]

[1]National Taiwan University

November 22, 2022

Abstract

In this study, the Superparameterized Community Atmosphere Model (SPCAM) is used to simulate tropical cyclones (TCs) using the hindcast approach. Three hindcast experiments are conducted with 32-km (D32), 128-km (D128), and 1024-km (D1024) horizontal scales in the sub-grid cloud-resolving models (CRMs). The results show that D1024 produces reasonable TCs compared with the reanalysis data. It is 3.42 TCs per 10 days for the reanalysis data, while there are 8.07, 4.88, and 3.73 for D32, D128, and D1024. The bias of overestimating TC numbers grows with decreasing CRM scale. The D32 experiment also produces stronger TCs with a higher precipitation rate and wind speed. The bias is highly related to the efficiency of adjusting convective instability in the sub-grid CRM. The D32 exhibits higher column-integrated water vapor under warm conditions compared with D1024, indicating its inefficiency in removing water vapor by the weaker convective mass fluxes in the small CRM scale. That is, the vertical transport of convection in a smaller horizontal scale will be restricted by stronger subsidence because CRM columns for compensating are limited. The distribution of accumulated convective instability is broader and more frequent in D32. As a result, large-scale precipitating systems tend to develop in D32, leading to a higher probability of TC genesis. This study highlights the importance of sub-grid configuration when estimating TC activities using SPCAM.

Journal of Advances in Modeling Earth Systems

Supporting Information for

Effects of the Horizontal Scales of the Cloud-Resolving Model on Tropical Cyclones in the Superparameterized Community Atmosphere Model

Kuan-Ting Kuo, Chien-Ming Wu, Wei-Ting Chen

Department of Atmospheric Sciences, National Taiwan University, Taipei, Taiwan

Additional Supporting Information (Files uploaded separately)

Caption for Movie S1

Introduction

Movie S1 presents original SPCAM hourly outputs from three experiments containing precipitation rate, outgoing longwave radiation, wind field at 850 hPa, and area of tropical cyclones diagnosed by the algorithm described in the manuscript.

Movie S1 . Animations of TCs for the experiments (a) D32, (b)D128, and (c) D1024. The color shading is the precipitation rate. The gray shading represents the outgoing longwave radiation. The arrows are the wind field at 850 hPa, and the bottom arrow scale presents the arrow length of 40 m s-1. TCs are circled by red contours. The initial condition is ERA5 reanalysis data at 00UTC on 7 September 2017.

Hosted file

`essoar.10512624.1.docx` available at https://authorea.com/users/537428/articles/599326-effects-of-the-horizontal-scales-of-the-cloud-resolving-model-on-tropical-cyclones-in-the-superparameterized-community-atmosphere-model

Kuan-Ting Kuo, Chien-Ming Wu†, Wei-Ting Chen

Department of Atmospheric Sciences, National Taiwan University, Taipei, Taiwan

†Corresponding author: Chien-Ming Wu (mog@as.ntu.edu.tw)

Key Points:

- The hindcast method is applied to evaluate the impacts of sub-grid convective processes on TCs in SPCAM.
- TC numbers in SPCAM with 1024-km CRM domain size matches reanalysis.
- The 1024-km CRM scale is efficient in removing water vapor by strong convective mass fluxes.

Abstract

In this study, the Superparameterized Community Atmosphere Model (SPCAM) is used to simulate tropical cyclones (TCs) using the hindcast approach. Three hindcast experiments are conducted with 32-km (D32), 128-km (D128), and 1024-km (D1024) horizontal scales in the sub-grid cloud-resolving models (CRMs). The results show that D1024 produces reasonable TCs compared with the reanalysis data. It is 3.42 TCs per 10 days for the reanalysis data, while there are 8.07, 4.88, and 3.73 for D32, D128, and D1024. The bias of overestimating TC numbers grows with decreasing CRM scale. The D32 experiment also produces stronger TCs with a higher precipitation rate and wind speed. The bias is highly related to the efficiency of adjusting convective instability in the sub-grid CRM. The D32 exhibits higher column-integrated water vapor under warm conditions compared with D1024, indicating its inefficiency in removing water vapor by the weaker convective mass fluxes in the small CRM scale. That is, the vertical transport of convection in a smaller horizontal scale will be restricted by stronger subsidence because CRM columns for compensating are limited. The distribution of accumulated convective instability is broader and more frequent in D32. As a result, large-scale precipitating systems tend to develop in D32, leading to a higher probability of TC genesis. This study highlights the importance of sub-grid configuration when estimating TC activities using SPCAM.

Plain Language Summary

Tropical cyclones are a destructive weather system for low- and mid-latitude coastal regions but are difficult for global models to simulate correctly. One reason is that tropical cyclones are sensitive to representations of convective processes in the model. We examine the effects of horizontal scales for convection to see the changes in tropical cyclones. The horizontal scale sets a limit on the degree of convection organization. For a smaller horizontal scale, tropical cyclones are more and generally stronger because wet and warm environments are more frequent to happen. These wet and warm environments can be caused

by the inefficiency of weaker convection to transport water vapor into the high atmosphere in the small scale.

1 Introduction

Tropical cyclones (TCs) are one of the most destructive weather systems for low- and mid-latitude coastal regions. Simulating TCs in general circulation models (GCMs) remains challenging, even for models with high enough resolutions. There is a large variability in simulated TC frequency among the GCMs (Roberts et al., 2020). Knutson et al. (2020) assess the confidence for future projection of TC activity from the literature. Their review shows a high or medium-to-high confidence level for the increase of TC precipitation rate for the 2 ℃ of global warming. For TC frequency, although GCMs usually project a decreasing trend with warming (e.g., Held and Zhao 2011), they argue that observational evidence for the frequency change is unclear. The model results may be caused by biases in simulating TCs and limitations in capturing interactions between TCs and their large-scale environment. Emanuel (2021) uses a downscaling technique on climate models and suggests an increasing trend of TC frequency for a warming climate. He is also concerned about the ability of climate models to simulate TCs. Thus, understanding the processes that influence TC frequency simulated in GCMs is essential for enhancing confidence in future climate projections.

Due to the limitation of horizontal resolution in GCMs, the sub-grid parameterization in GCMs contributes to the uncertainty in simulating TC frequency. Villafuerte et al. (2021) showed that different convective parameterizations could cause significant differences in TC numbers from 1.2 to 22.5 TCs per year. In addition to directly changing convective schemes, reducing physics timestep can cause more TC numbers through decreased CAPE removal by convective parameterization and compensated grid-scale vertical mass flux (Zarzycki 2022). Zhao et al. (2012) show that the TC frequency is sensitive to model parameters such as cumulus lateral mixing rate and divergence damping. These studies suggest that conventional parameterizations have significant impacts on TC frequency. However, evaluating the correctness of parameter tuning is difficult. Parameter tuning without examining the sub-grid processes may cause overfitting to the present climate and give a wrong projection for future climate. Therefore, we took the convective permitting approach with a superparameterized GCM to tackle this problem.

Superparameterization (SP) refers to the sub-grid representation that the cumulus parameterization in each grid column is replaced by a nested integration of two-dimensional cloud-resolving models (CRMs) to simulate convection explicitly at the given grid-scale tendencies. SPCAM is a GCM with SP developed by Khairoutdinov and Randall (2001) based on the Community Atmosphere Model (CAM) from the National Center of Atmospheric Research (NCAR). Previous studies have reported improvements in simulating diurnal variation of rainfall (Khairoutdinov et al. 2005; Zhang et al. 2008; Pritchard and Somerville 2009), Madden-Julian Oscillation (Benedict and Randall, 2009), low-level moistening

before major precipitation events (DeMott et al. 2007), and Asian summer monsoon mean state (DeMott et al. 2011). The South China Sea summer monsoon, a sub-system of the Asian summer monsoon, has been investigated with this model (Kuo, Chen, and Wu 2020). With these improvements, SPCAM is suitable for investigating the multiscale weather systems when convection plays an important role. On the other hand, it is well known that SPCAM tends to produce precipitation hotspots over the Asian summer monsoon region and the western North Pacific in climate simulations (Khairoutdinov et al., 2005; Randall et al., 2016). Such bias may be partially related to tropical cyclones. Therefore, in this study, we will use SPCAM to explore model sensitivities in simulating TC activities over the western North Pacific.

GCM with SP can explicitly calculate cloud-scale statistics from CRMs without diagnosing the grid-scale environment with physical or empirical assumptions. In this case, different CRM configurations may tend to generate specific cloud distributions or convective characteristics. In an early sensitivity test, Khairoutdinov and Randall (2001) examined four configurations with an 18-day simulation in a CRM (which is implemented in SPCAM). They conclude that the changes in the geometry (2D or 3D), the domain size, and the resolution do not cause any clear bias, and all experiments perform consistently. However, this study only tests CRM performances with prescribed large-scale forcing. The interaction between the large-scale and the sub-grid parameterization is not included. More recently, Cheng and Xu (2014) focused on the orientation of the 2D CRM based on three types of environments for the mesoscale convective systems (MCSs). Their results showed improvements in reducing biases of precipitation and circulation. Pritchard et al. (2014) tested the effects of horizontal scales on the Madden-Julian Oscillation (MJO). They conducted three experiments for 32, 64, and 128-km CRM domain sizes. They concluded that the CRM horizontal scales are not critical to MJO dynamics in SPCAM, but the shortwave cloud forcing is enhanced for the smaller CRM domain size in the tropics. Tao and Chern (2017) focused on the resolutions and grid points of CRMs for the ability to simulate MCSs. Their result indicated that only higher resolutions (1 km or 2 km) and more grid points (128 and 256) could simulate realistic MCSs. This improvement also affected the Hadley circulations and precipitation patterns. These studies show differences among configurations which can cause varying degrees of influence on different weather systems. So, the configurations can be viewed as different types of the sub-grid convective property. In addition, SPCAM has been used in recent studies to develop machine learning based convective parameterization (Gentine et al. 2018; Rasp et al. 2018; Mooers et al. 2021), as the simulations provide realistic convective variability within the CRM under various large-scale environments. However, these studies used simulations with a specific CRM configuration. It is worth exploring how different types of sub-grid convection can produce different relationships with the large-scale environment, particularly in the more extreme cases such as grid-scale TC activities.

There are multiple approaches of experimental design to examine the effects of

sub-grid configurations on TCs in SPCAM. A straightforward way is to run a set of long-term climatology experiments and diagnose the number of TCs or other TC statistics. However, long-term experiments may produce very different states of the large-scale circulation. In this condition, the change in TC statistics involves both the sub-grid effects of convection characteristics and the variabilities of the large-scale environment. Therefore, to evaluate only the impacts of sub-grid convective processes on TCs, we choose the short-term hindcast approach following Ma et al. (2013, 2021). They showed that the short-term hindcast approach could diagnose the systematic bias caused by the fast moist processes in a few days by directly comparing with the observations/reanalysis. Patricola and Wehner (2018) used the hindcast method to simulate selected TC events and assessed anthropogenic influences by the pre-industrial condition and future projection forcing. Most of the intense TCs were getting stronger in the future warming climate, and the change of TC intensity between the past and present climate was insignificant. The short-term hindcast approach preserves a similar large-scale environment to the initial conditions so that the sensitivity experiments are comparable with the observation through diagnosing the fast moist convective processes in the sub-grid. Therefore, here we will carry out SPCAM hindcast experiments to evaluate the TC frequency under different CRM horizontal scales. The paper is organized as follows. Section 2 describes the model and experiment design, including the hindcast setup and TC detection algorithm. The simulation and analysis results are presented in section 3. Section 4 provides the summary and discussion.

2 Methodology

2.1 Model and Experiments

The model used in this study is superparameterized CESM version 1.1.1. To simulate TCs in SPCAM, we use $0.9°\times1.25°$ horizontal resolution and 30 levels in the vertical. The CRM resolution is 4 km with a periodic boundary condition, and the microphysics scheme is a single-moment scheme (Khairoutdinov and Randall, 2003; Khairoutdinov et al., 2005). The sensitivity of the coupling between convection and the large-scale environment is assessed by modifying the horizontal domain size of the sub-grid CRM. Three experiments are conducted by using domain sizes of 32, 128, and 1024 km with a 4-km horizontal resolution, and are denoted as D32, D128, and D1024, respectively. These experiments represent the degrees of the lateral boundary constraints for convection to develop. The larger domain size is expected to allow a broader cloud spectrum or a more intense convective cloud to develop in a single timestep.

2.2 Hindcast setup

The hindcast experiment is initiated each day from June-September 2017 (122 initializations), and the model is integrated for 10 days in each experiment, simulated for a total of 1220 days. The initial conditions are created from the fifth generation ECMWF atmospheric reanalysis (ERA5; Hersbach et al. 2020). The sea surface temperature (SST) and sea ice are prescribed by Optimum Interpo-

lation SST (OISST) version 2.1 (Huang et al. 2021). The hindcast approach allows direct comparison with observation data. The first to the last day is denoted as Day 0 to Day 9 in each hindcast simulation. An ensemble average from a specific hindcast day (e.g., an average of Day 0 from all 122 simulations) can represent the 2017-summer average with a certain degree affected by the initial conditions. That is, the ensemble averages from Day 0 to Day 9 represent the results/biases transitioned from initial-condition dominating to model-intrinsic dominating by comparison.

Because the experiments use ERA5 as the initial conditions, we also separate ERA5 into the 122 10-day hindcast periods as the validation data. The same procedure is also applied to the Global Precipitation Measurement (GPM) IMERG product as the precipitation validation data (Huffman et al., 2019).

2.3 Algorithm for tropical cyclones

To properly identify TCs in SPCAM, we adopt the definition from Oouchi et al. (2006) with additional conditions adjusted to identify TCs from ERA5 better. All criteria are listed as follows:

(1) The minimum sea-level pressure is at least 2 hPa lower than the average surface pressure over the surrounding 7° x 7° grid box.

(2) The magnitude of the maximum relative vorticity at 850 hPa exceeds 3.5 x 10^{-5} s^{-1}.

(3) The maximum wind speed at 850 hPa is larger than 15 m s^{-1}.

(4) The maximum wind speed at 850 hPa is larger than that at 300 hPa.

(5) The duration is not shorter than 36 hours.

(6) The surface pressure is lower than 1008 hPa.

(7) The object is excluded when the minimum surface pressure is lower than 880 hPa over the surrounding $5^\circ \times 5^\circ$ grid box.

(8) At least for one timestep, the SST is higher than 26 ℃.

All grids that satisfy the criteria and neighbors are connected and tracked by a tracking method from Moseley et al. (2019). The criteria (1)-(5) are the same as Oouchi et al. (2006). The criterion (6) guarantees the minimum strength of TCs. The criterion (7) can help filter out the topography. The criterion (8) restricts the tracks to those passing through tropical oceans so that extratropical cyclones are excluded. These same criteria were applied to both SPCAM experiments and the ERA5 data with the exact resolution for a fair comparison. Figure 1 illustrates TCs diagnosed by this algorithm from the ERA5 data from 28 July 2017 to 5 August 2017. There were four typhoons during this period. This algorithm can detect the exact TC events. There are still some rare events that can complicate the TC track identification. For example, Typhoons Haitang and Nesat merge into one TC by the algorithm at 01UTC 30 July, then split after 3 hours. This merge and split behavior may cause TC track shifting but will

not affect TC numbers and TC areas, which will be analyzed in the following sections. The TC areas circled by color contours are the grids that pass the TC algorithm, and the TC tracks are the lines connecting the center of the TC areas.

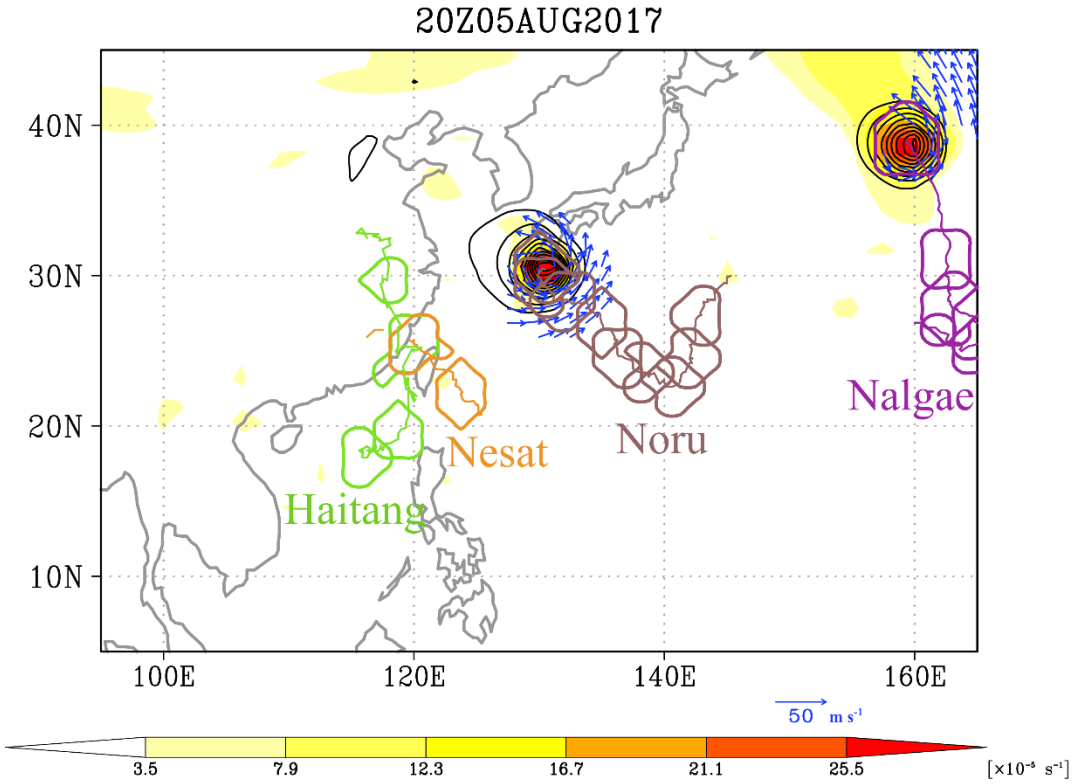

Figure 1. TCs diagnosed by the TC algorithm using ERA data. The shading is relative vorticity. The blue arrows are the wind field at 850 hPa and the magnitude stronger than 15 m s^{-1}. The black contour is sea-level pressure from 1000 hPa with a 2-hPa interval. The color contours and lines present TCs from 28 July 2017 to 5 August 2017. The interval of color contours is 24 hours. The names of TCs are labeled below the paths.

3 Result

3.1 TC precipitation

Figure 2 shows the ensemble average of TC precipitation over the western North Pacific along the hindcast days. Each hindcast day represents the 2017 summer average with a few different days (e.g., 20170601 to 20170930 for Day 0, and 20170610 to 20171009 for Day 9) depending on the elapsed days of the simula-

tions. The figure shows a systematic bias associated with the CRM horizontal scales. On Day 0, all experiments are close to the observation/reanalysis. However, in the later hindcast days, all experiments produce higher precipitation than the observation. Among the experiments, D32 increases the most. The precipitation is over 0.3 mm h^{-1} higher than the GPM observation on Day 8. For D1024, the bias is less than 0.05 mm d^{-1} compared with the observation through the hindcast days. D1024 also exhibits a gentler change, while precipitation in D32 and D128 sharply increases before Day 7. This increase can be contributed by more TCs or/and more intense rainfall by a single TC. Before analyzing the overall precipitation difference among the experiments, we will first demonstrate a TC case to understand the TC simulations on different hindcast days.

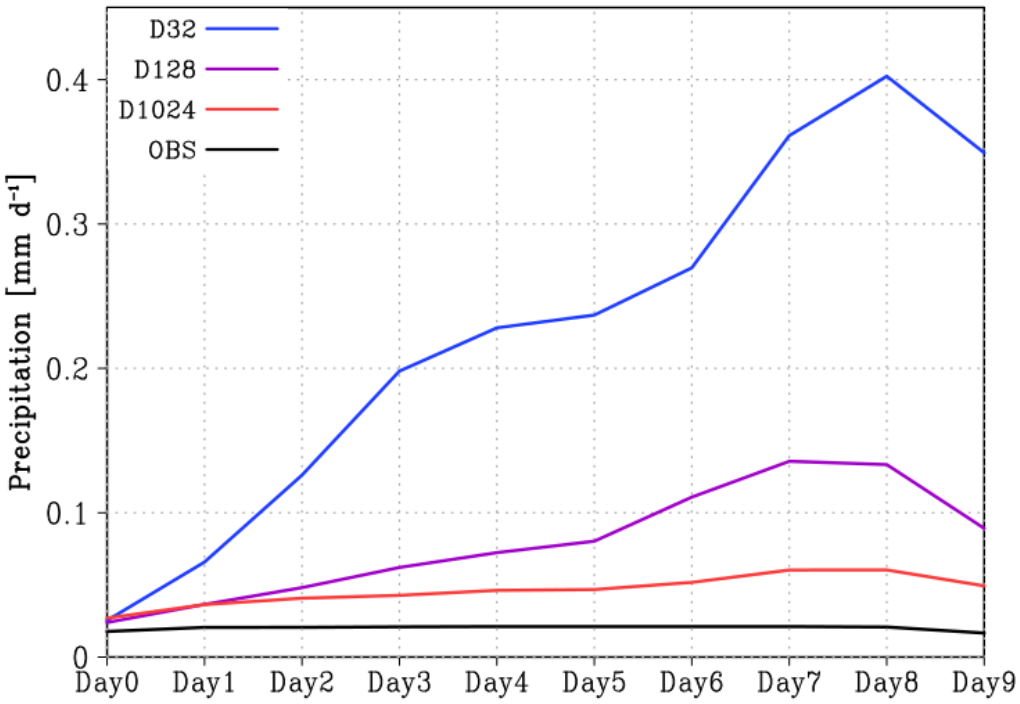

Figure 2. The ensemble average of TC precipitation over the western North Pacific (0 ° - 40 ° N, 100 ° E - 180 ° E) by each hindcast day. The blue, purple, and red lines represent experiments D32, D128, and D1024, respectively. The black line is observation, where precipitation is from the GPM, and TC areas are diagnosed from ERA5 data.

3.2 A case study for Talim typhoon

With the hindcast approach, we can directly compare the performance of TC simulation in each experiment with a real TC case. Here, we choose Typhoon Talim over the western North Pacific as an example. According to the best track data from the Japan Meteorological Agency (JMA), Typhoon Talim was detected as a tropical depression at 20170908 12Z and strengthened into the typhoon category at 20170911 18Z. Figure 3 shows tracks of Typhoon Talim from ERA5 and in the experiments identified by the closest TC within 900 km to the center of Typhoon Talim at 20170911 18Z, the location with a typhoon symbol. The criterion of 900 km is selected to avoid choosing Typhoon Doksuri, which locates around the south of Typhoon Talim. The initial date 20170907 is selected to analyze because it is the earliest initialization when Typhoon Talim can be identified during the 10-day integration in all experiments. Animations in this period are provided in movie S1. Figure 4 shows the maximum wind speed at 850 hPa and precipitation rate within the area defined as Typhoon Talim. Typhoon Talim is detected earlier in D32 than in D128 and D1024. For D32, it intensifies faster at the early stage. When strengthened into the typhoon category, the maximum precipitation is 22 mm h^{-1} for D32 while only 6 mm h^{-1} for D1024. The maximum wind speed is 29.7 m s^{-1} for D32 while 18.2 m s^{-1} for D1024. This result shows that, for Typhoon Talim, D32 intensifies earlier than in the other two experiments and produces more rainfall. Although the TC in D128 and D1024 further intensifies at the later stage, the tracks and environments vary among the experiments (Fig. 3). It may not be suitable to compare experiments directly.

This case study shows clear systematic differences in wind speed and precipitation for the experiments for the first four hindcast days. There are, however, internal variabilities later in the simulations. Therefore, the following comparison will focus on the experiments' overall statistics for all tropical cyclones.

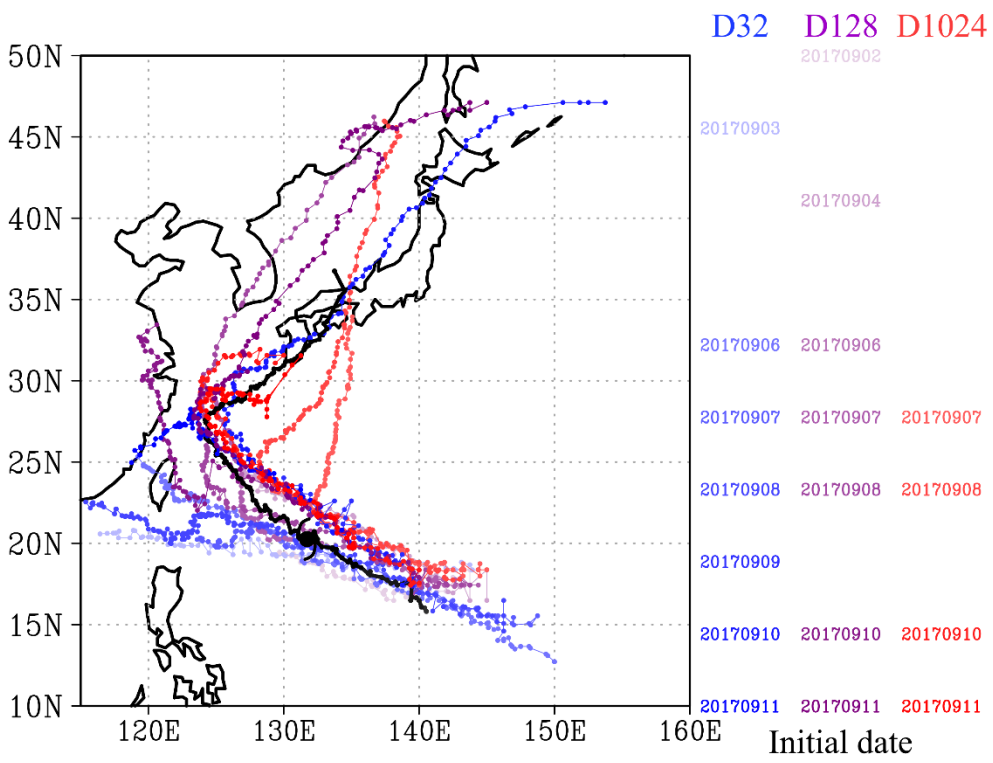

Figure 3. Diagnosed tracks of Typhoon Talim (2017). The red, purple, and red colors are experiments D32, D128, and D1024, respectively. The black color represents the diagnosed track from ERA5. The colors from light to dark represent the hindcast initial date from early to late.

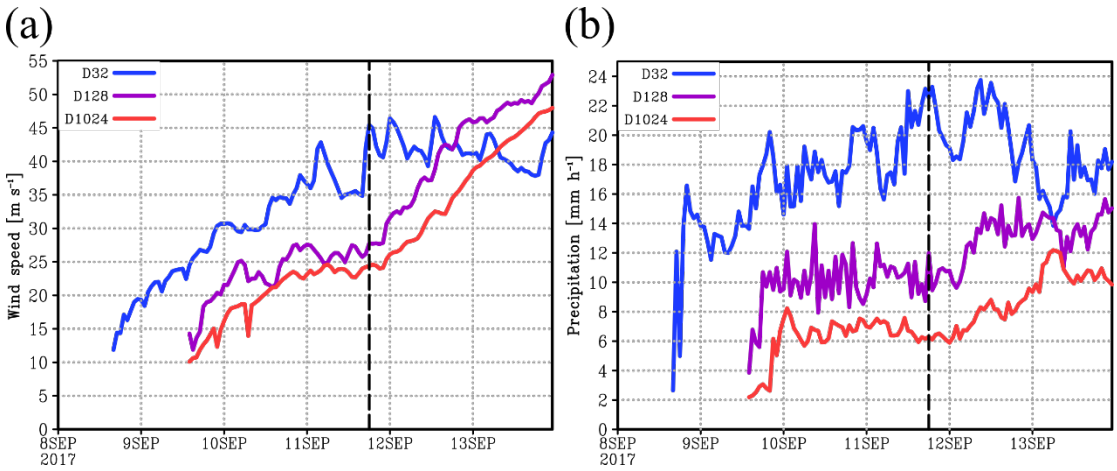

Figure 4. The hindcast runs initialed on 7 September 2017 of (a) maximum wind speed at 850 hPa and (b) maximum precipitation within Typhoon Talim. The dashed line illustrates the time of 18Z 11 September 2017, when Typhoon Talim intensified to typhoon category by the best track data from the Japan Meteorological Agency.

3.3 TC statistics

Table 1 lists the TC numbers and lifetimes in all experiments and the reanalysis data. ERA5 data is regridded to the same horizontal resolution as the SPCAM and splits into 122 hindcast cases like the experiments. On average, 8.07, 4.88, and 3.73 TCs formed per 10-day simulation in D32, D128, and D1024, respectively, while only 3.42 TCs are diagnosed from ERA5. TC lifetimes are not significantly different among the three experiments. They are all shorter than ERA5 by about 10 hours.

Although D32 generates twice more TCs as D1024, the strength of the TCs is not weaker. Figure 5 shows the maximum 850-hPa wind speed and the maximum precipitation rate for each TC. The wind speed is higher in D32 than in D128 and D1024, and the spread (full range and interquartile range) is also more extensive. The precipitation rate shows a more significant difference among the three experiments. D32 can produce precipitation over 30 mm h^{-1}; the average is over 5 mm h^{-1} higher than D128 and D1024. This result implies that the environment in D32 is more favorable for TC genesis and development.

For spatial distribution (Fig. 6), all SPCAM experiments can generate TCs in the southern Indian Ocean which does not exist in ERA5. The experiments also have too many TC tracks around the central North Pacific, while there is no TC track in the observation. This bias is weaker in D128 and D1024 and most severe in D32. In the South China Sea and the eastern Pacific, the TC track density of D32 is over 50 hours higher than the others. This result represents that D32 produces more TCs probably because of wider spatial distribution and higher occurrence frequency of TCs. It also explains why D32 produces more

TC precipitation over the western North Pacific (Fig. 2).

Table 1. TC statistics of ERA5, D32, D128, and D1024

Exp.	ERA5	D32	D128	D1024
Total TC number	417	985	595	455
Number per 10 days	3.42	8.07	4.88	3.73
Average lifetime [hr]	103.81	95.22	90.54	95.85

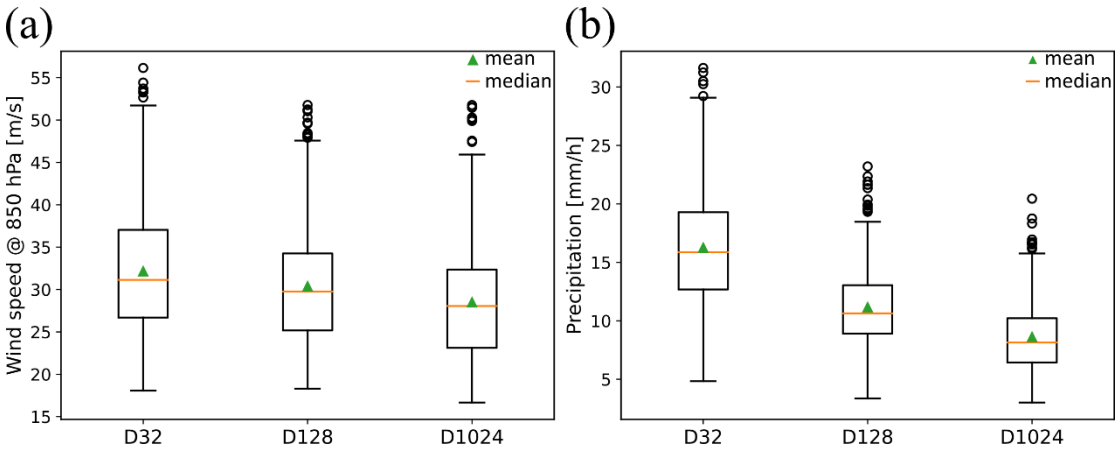

Figure 5. box plots of (a) Maximum wind speed at 850 hPa and (b) maximum precipitation for all TC events.

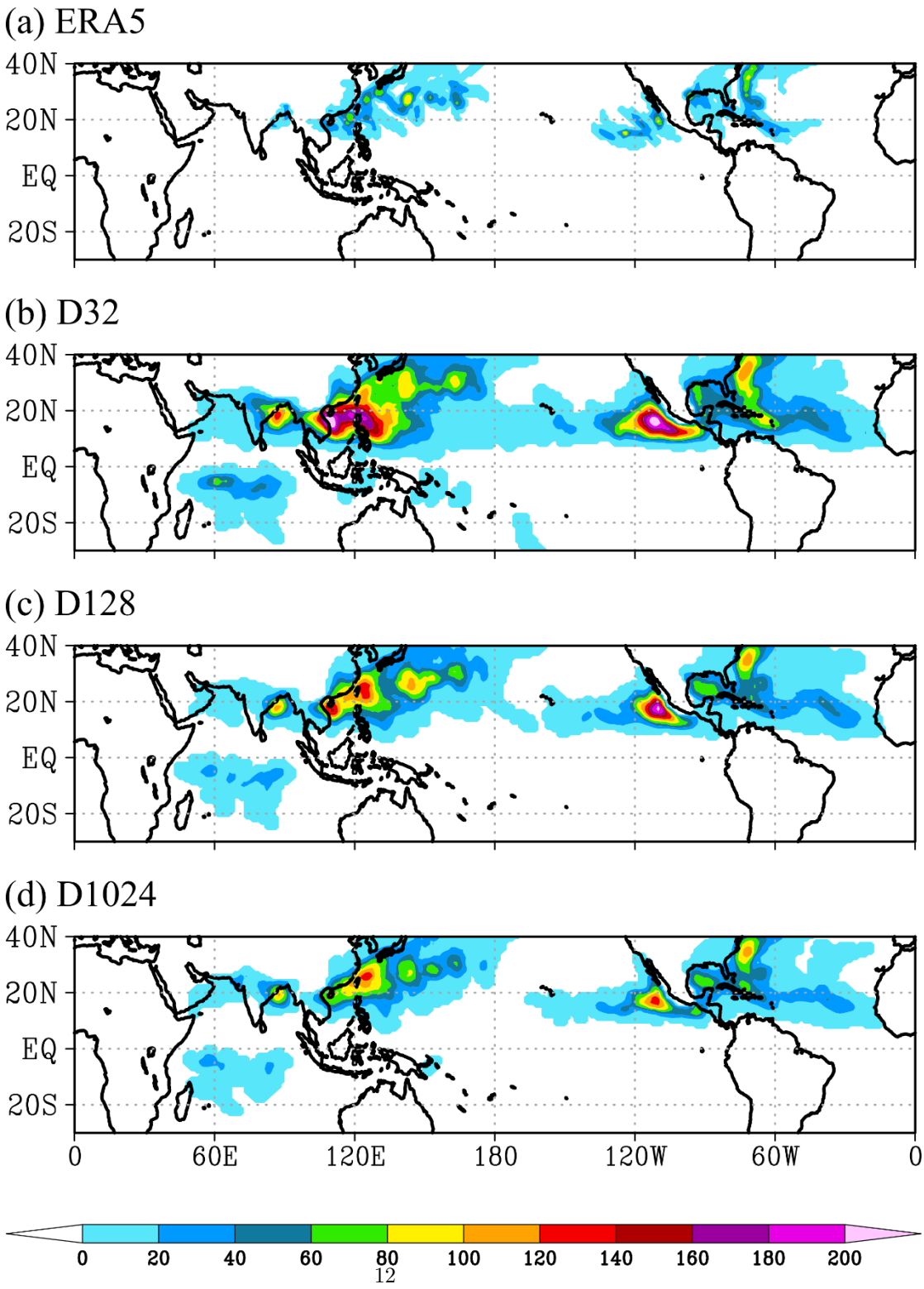
(a) ERA5
40N
20N
EQ
20S
(b) D32
40N
20N
EQ
20S
(c) D128
40N
20N
EQ
20S
(d) D1024
40N
20N
EQ
20S
0
60E
120E
180
120W
60W
0
0
20
40
60
80
100
120
140
160
180
200

Figure 6. The ensemble average TC track density on the TC areas for (a) ERA5, (b) D32, (c) D128, and (d) 1024. The TC areas are defined as circled areas in Fig. 1. The unit is hours per summer (June - September).

3.4 Moisture Bias

TC genesis and TC tracks can be affected by many factors. The most well-knowns are SST, vertical wind shear, vertical instability, environmental vorticity, and humidity. Given our hindcast approach, some of these factors do not affect or play a minor role when explaining the difference in TC genesis among the experiments. For example, SST is prescribed for all experiments, and the large-scale environment changes little for 10-day hindcast experiments. The convective process is the most critical process to take effect significantly in a short period.

A relative convective bias of SPCAM has been reported by Kuo and Neelin et al. (2020). They assessed model biases of convective parameterization by diagnosing precipitation rate as a function of CWV and averaged tropospheric temperature (T_{ave}; equivalent to column-integrated saturation humidity in their paper). Their results show that the pickup line of SPCAM for precipitation exhibits a gentler slope for higher T_{ave}, and the CWV probability density functions (PDFs) extend to a high CWV regime for high T_{ave}. At the same time, it is close to observation for low T_{ave}. Their results imply that SPCAM is less efficient in removing moisture in the troposphere under warm conditions. We apply the same analysis technique to our experiments and focus on the CWV PDFs.

Figure 7 shows the CWV PDFs for observation and the three experiments in the western Pacific, the eastern Pacific, the Atlantic, and the Indian Ocean bounded by 20 $^\circ$S and 20 $^\circ$N. The colors represent different T_{ave} conditional samplings. For observation, in the western Pacific (Fig. 7a), the CWV PDFs increase rapidly when CWV is between 10 and 30 mm. Then, the PDFs slowly increase (decrease) for high (low) T_{ave}. When CWV is high enough, the PDFs drop sharply, meaning water vapor is removed quickly. More discussion about these decline lines and their relationship with T_{ave} can be found in Kuo et al. (2018). The CWV PDFs in other ocean basins (Figs. 7e,i,m) are similar to those in the western Pacific. Only the counts of T_{ave} sampling vary among the four basins, corresponding to the higher or lower peaks in the shapes of their PDFs. The dashed lines in Fig.7 roughly illustrate the upper bound of CWV PDFs for $T_{ave} > 271$ K in each ocean basin in observation. If a CWV PDF extends to a higher CWV regime, it means that the environment is wetter on average under the T_{ave}. Kuo and Neelin et al. (2020) mentioned a high CWV extending bias in SPCAM with a similar CRM setting as D128 except for the vertical 24 levels. Although this bias still exists in our experiment (Figs. 7c,g,k,o), the performance is better as here the extension is less than their result. This improvement can be related to higher GCM resolution ($2.5^\circ \times 1.9^\circ$ resolution in their model setting) or more vertical levels.

This moist bias becomes severe in D32 across the ocean basins (Figs. 7b,f,j,n),

and there are unrealistic PDF peaks for CWV higher than the observation. In the Atlantic, for example, Fig. 7j exhibits a clear bifurcation for 273 K, and the CWV of a PDF peak is higher than the upper bound of observation (i.e., the dashed line). The dip in the CWV PDF indicates an unstable environment. If an environment favors the accumulation of CWV (e.g., low-level moisture convergence), the CWV will increase rapidly. The CWV PDFs in the western and eastern Pacific exhibit the same bias, but the bifurcation is weaker at 274 K and 273 K, respectively (Figs 7b,f). In the Indian Ocean, the bias of CWV PDF extending into the moister condition still exists, but the bifurcation is unclear.

On the other hand, D1024 performs better than D32 and D128. The upper bound of CWV PDFs is close to observation in the eastern Pacific and Atlantic (Figs 7h,l). For the western Pacific and the Indian Ocean, the upper bounds are close to observation, but the peaks of CWV PDFs are lower, so the slopes are flatter than the observation (Figs. 7d,p). Generally speaking, the moist CWV bias in D1024 is small. The only caveat is the deviation for T_{ave} =275 K in the western Pacific (Fig. 7d), and the event counts for this condition is low in the observation (probability $< 10^{-5}$).

The CWV PDFs reveal a significant moisture bias of high CWV under high T_{ave} conditions for D32. On the other hand, D1024 shows relatively reasonable CWV PDFs among all experiments. This result implies that D32 is less efficient in adjusting convective instability. In the following subsection, we will focus on the spatial distribution of the event of high CWV under high T_{ave}.

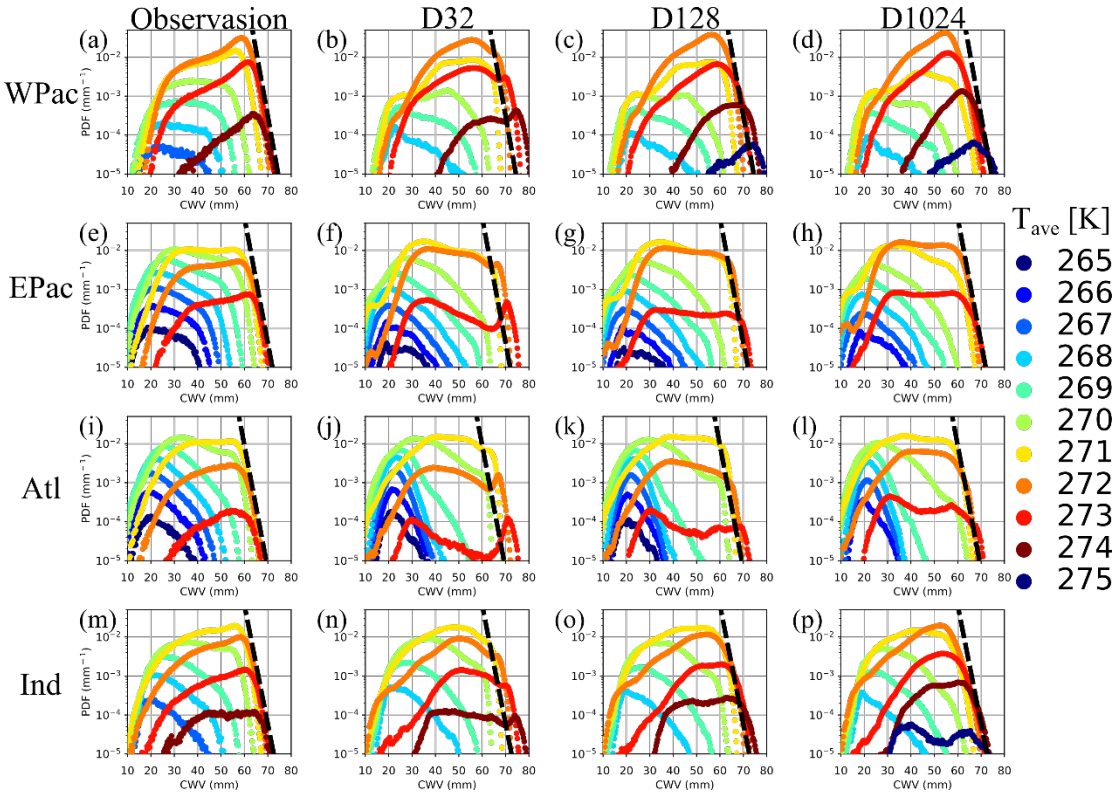

Figure 7. CWV PDFs for (a)(e)(i)(m) observations and experiments of (b)(f)(j)(n) D32, (c)(g)(k)(o) D128, and (d)(h)(l)(p) D1024 over (a)-(d) the Western Pacific, (e)-(h) the Eastern Pacific, (i)-(l) the Atlantic, and (m)-(p) the Indian Ocean within 20 ° S and 20 ° N. The colors mark the conditional samplings by the tropospheric temperature averaged between 1000 hPa and 200 hPa. The dashed lines illustrate the decline lines of the PDF in the observations in each ocean basin.

3.5 High T_{ave}-high CWV events and TCs

SPCAM exhibits unrealistic high CWV under high T_{ave} conditions, especially for experiment D32. Under these high T_{ave}-high CWV regions, TCs should be one of the most efficient weather systems to consume moisture and maintain high T_{ave} with a warm core structure. Figure 8 examines the occurrence probability for $T_{ave} > 271$ K and CWV > 70 mm and the probability of these events related to TCs. The left panel shows the spatial distribution of the probability of the high T_{ave}-high CWV events. These events occur most frequently in the Bay of Bengal in both the experiments and the observation. Other regions shown in the observations include the eastern Arabian Sea, the western North Pacific, and the North Atlantic. The SPCAM simulations exhibit similar distribution but cover broader areas in the experiment with smaller CRM scales. These

areas are identical to the areas with a significant bias of TC track density (Fig. 6), including the South China Sea, the southern Indian Ocean, and the eastern North Pacific, and more severe for D32 in the central Pacific. The consistent spatial distributions imply a possible relationship between the high T_{ave}-high CWV events and TCs.

The right panel of Fig. 8 depicts the occurrence probability of TCs while the high T_{ave}-high CWV events occur. The high T_{ave}-high CWV events are usually related to TCs in the western North Pacific and the North Atlantic in the observation. In the North Atlantic, this feature is consistent throughout all experiments. However, this relationship is weaker for the experiments with smaller CRM domain sizes over the western North Pacific. The difference between the North Atlantic and the western North Pacific may be related to a difference in the specific mechanisms of TC genesis. The environment in the North Atlantic is generally dryer and colder than in the western North Pacific. The TC genesis in the Atlantic is primarily related to the easterly wave, so the high T_{ave}-high CWV events are a result of TC-induced moisture convergence and convective heating. In contrast, the TC genesis in the western North Pacific is more complicated, involving other weather systems like the MJO (Liebmann et al. 1994) and the summer monsoon (Wu et al. 2011). Besides, the moist and warm environment in the western North Pacific usually causes high convective instability. Therefore, TC can be the cause or the result of the high T_{ave}-high CWV events in the western North Pacific.

Another viewpoint is that the high T_{ave}-high CWV events should only happen under strong convergence conditions like TCs. A larger CRM domain can consume water vapor more efficiently through deeper convection and the accompanied strong subsidence, so only strong low-level water vapor convergence can accumulate CWV and maintain high T_{ave}. For smaller CRM domains, convection could be less efficient in consuming water vapor, so CWV can quickly accumulate even under weak convergence conditions. To further investigate the low efficiency of convection in D32, we next examine the average mass fluxes for convective clouds in the experiments.

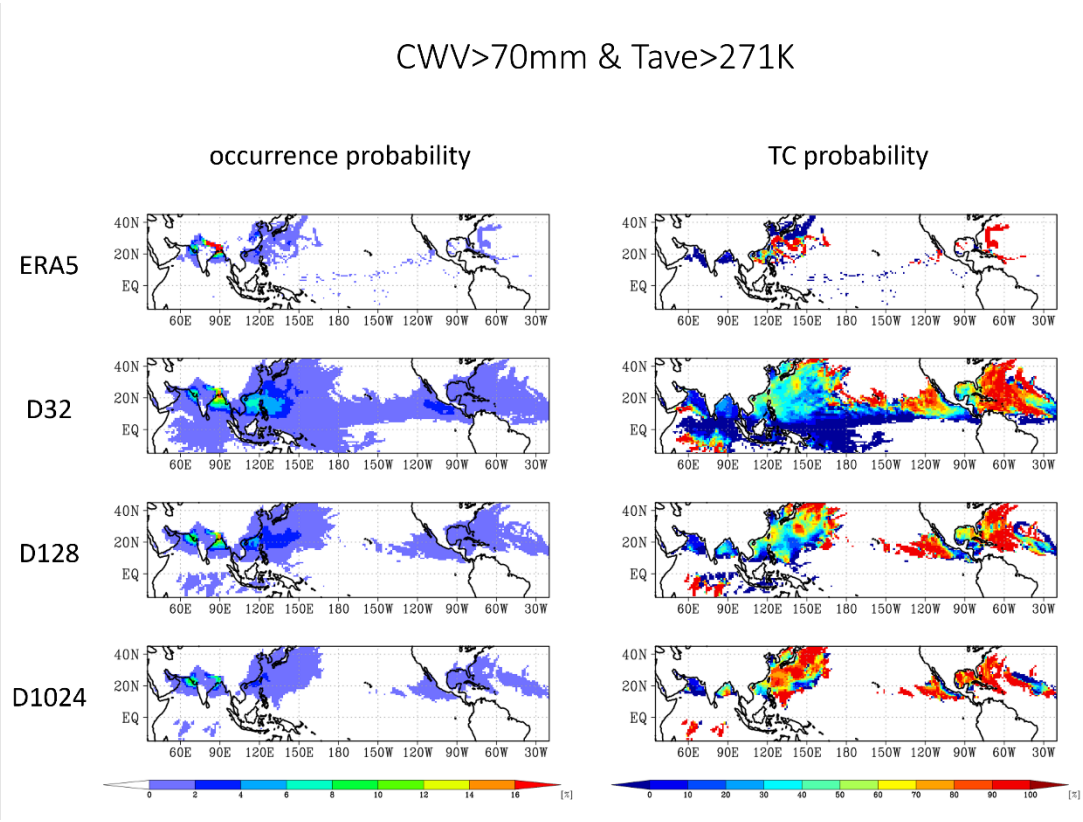

Figure 8. The left column is the occurrence probability for CWV > 70 mm and T_{ave} > 271 K. The right column is the occurrence probability of TCs under the high CWV and T_{ave} conditions.

3.6 Convective clouds in CRMs

The mass fluxes can help explain the environmental difference for convective clouds in different CRM domain sizes. We define convective clouds as the mixing ratio of cloud water and cloud ice is more than 10^5 kg kg^{-1} for all levels within 2 km to 6 km, and the vertical velocity is higher than 1 m s^{-1}. Figure 9 shows the average mass flux and cloud top height of convective clouds in each experiment. The strongest mass flux and highest convective cloud top are simulated in D1024, and D32 exhibits the weakest mass flux and the lowest convective cloud top. This result shows that the horizontal scale can influence the development of convective clouds. The smaller domain size limits convection development and causes weaker vertical transport and a lower convective cloud top. The mass flux difference is summarized in the schematic diagram in Fig. 10 for cloud distribution in the CRMs between D1024 and D32 under a convective condition. For D1024, more convective clouds can exist simultaneously, and strong convection can extend deeper into the tropopause. In contrast, D32 can only contain

one or a few convective clouds; the strength is weak, and the cloud top height is low. If the domain is not sufficiently large, a convective cloud will suppress itself for further development by the compensating downdraft. Therefore, the domain size will constrain the strength of convection, causing low efficiency for water vapor in the boundary layer to be transported into the mid-troposphere and above. More water vapor will, therefore, accumulate within the boundary layer for the small CRM domain size, leading to higher CWV on average. Pritchard et al. (2014) also mentioned a similar effect. Their result emphasized on the difference in low clouds, while our result reveals the impact on convective clouds.

The low efficiency of sub-grid convection in consuming convective instability implies that D32 needs additional large-scale forcing in the GCM scale to help release the convective instability. So, TCs play this role. In the SP framework, however, this increased instability can only be advected because convective processes can only exist in the sub-grid. Therefore, convective processes cannot quickly adjust the high CWV bias for the experiment with a small CRM domain. Eventually, D32 exhibits more events and broader distribution for high T_{ave}- high CWV.

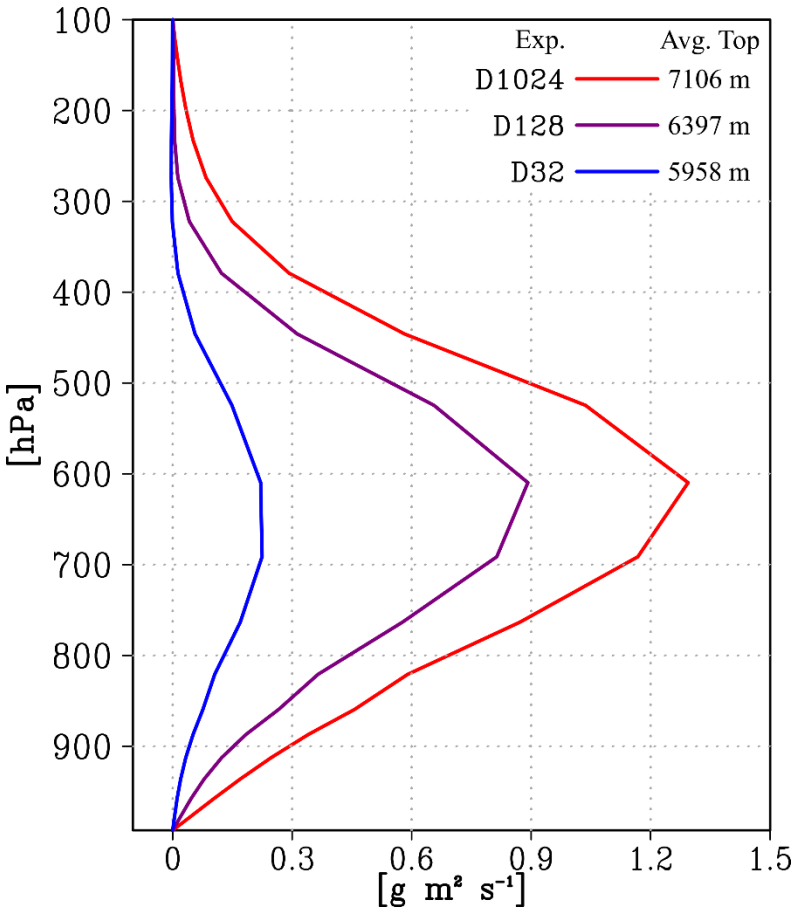

Figure 9. The mean mass fluxes for convective clouds. The convective clouds are defined as cloud water plus cloud ice $> 10^{-5}$ kg kg^{-1} for all levels within 2 km to 6 km, and vertical velocity > 1 m s^{-1}. The average convective cloud top height is labeled at the upper right corner for each experiment.

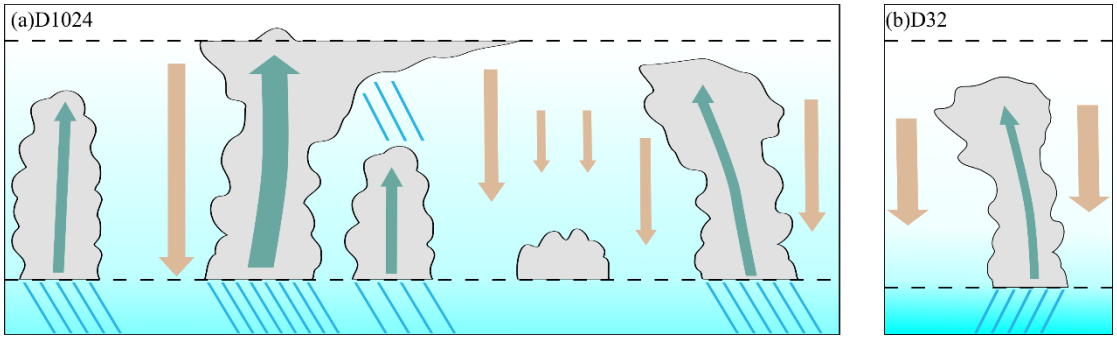

Figure 10. A schematic diagram adapted from a snapshot of the experiments

(a) D1024 and (b) D32. The blue shading represents the water vapor mixing ratio. The green arrows represent the updraft of convection. The yellow arrows represent the compensating subsidence to convection. The bottom and top dashed lines represent the boundary layer and the tropopause, respectively.

4 Summary and Discussion

This study carried out a set of hindcast experiments using SPCAM to examine the effects of sub-grid convection processes on TC statistics. A clear difference in the number of simulated TCs can be identified among three experiments for 32-, 128-, and 1024-km horizontal scales in CRMs of the SPCAM. More numerous and more tensed TCs are generated in the configuration with a smaller CRM domain size. To further link the changes in TC statistics to the sub-grid convective processes, we examined the CWV PDFs. There was a more severe moisture bias in D32 than in the other two experiments with a larger CRM domain, with more frequent high CWV events under warm tropospheric temperature conditions, leading to a very different relationship among CWV, temperature, and TCs. The statistics revealed the inefficiency to consume water vapor by convection when the CRM domain is small. This domain size dependence is also identified in the average convective mass fluxes, and the experiments with larger domain sizes exhibit stronger mass fluxes.

Naturally, TCs can be tightly associated with high T_{ave}-high CWV events. However, most high T_{ave}-high CWV events in D32 are not related to TCs, in contrast to their high correlation in D1024. This implies that most high T_{ave}-high CWV events in D1024 are induced by TCs, while D32 produces warmer and wetter environments more frequently due to the inefficient sub-grid water vapor removal, which is not directly related to TCs. We demonstrate that the larger CRM domain size exhibits more realistic CWV removal than the smaller one. This bias quickly accumulates in D32 because CWV can only be removed through the sub-grid processes under the SP framework. As a result, the frequent occurrence of high convective instability regions leads to more numerous TC genesis and development.

Our results also have an important implication for the convection parameterization based on SPCAM outputs using the machine learning method. Although the cloud-resolving approach captures the variability in convective structure more realistically than conventional parameterization, the results obtained in this study suggest that more variability can be generated by the CRM model configurations, especially in the extreme events such as tropical cyclones due to the strong convection-large scale interactions. For parameterization based on machine learning, the additional combination of convection-large scale environment samplings provide the scenario for learning such interactions. This echoes Jones et al. (2019a; 2019b) that an ensemble approach is needed for the SP-CAM to better represent climate variability. In addition, model physics in the embedded CRM can also play a role in modulating the convection-large-scale interactions. Huang and Wu (2020) demonstrated that even under a strong large-scale forcing, the simulated precipitation spectrum can be different when

different microphysics schemes are adopted.

Although we demonstrate many benefits of using a larger CRM domain size, there are some non-improving biases. For example, D1024 exhibits a poleward shift of ITCZ and SPCZ, causing an obvious precipitation pattern bias. This problem may involve circulation shifted by inhomogeneous energy distribution, Kuo, Chen and Wu (2020) demonstrated that monsoon simulations with the SP-CAM can be improved when coupled to a slab ocean model. Following their studies, we will test the performance with a 1024-km CRM domain size and slab ocean model to understand the relationship between tropical cyclones and the large-scale circulations related to the western north pacific monsoon, with the consideration of air-sea interactions.

Acknowledgments

K. Kuo is supported by the Elite Doctoral Scholarship from the National Science and Technology Council of Taiwan (NSTC) and National Taiwan University. C. Wu is supported by NSTC111-2111-M-002-012, Academia Sinica (ASTP-109-M11), and Ministry of Education (111L7840). W. Chen is supported by NSTC109-2628-M-002-003-MY3. We thank to National Center for High-performance Computing (NCHC) for providing computational and storage resources.

Open Research

The processed data and codes for each experiment and reanalysis/observation are available at https://doi.org/10.5281/zenodo.7156318. The data is categorized by experiments and initial dates. The codes for analysis and visualization are available for these data. The raw data of simulation outputs are available for online sharing upon request due to the large volume of the dataset.

The SPCAM code is available at https://svn-ccsm-release.cgd.ucar.edu/model_development_releases/spcam2_0-cesm1_1_1. The tracking algorithm for identifying an individual TC event is available at https://github.com/christophermoseley/iterative_raincell_tracking. The code for CWV PDFs is available at https://github.com/NOAA-GFDL/MDTF-diagnostics/tree/main/diagnostics/convective_transition_diag.

References

Benedict, J. J., & Randall, D. A. (2009). Structure of the Madden–Julian Oscillation in the Superparameterized CAM. *Journal of the Atmospheric Sciences*, *66*(11), 3277–3296. https://doi.org/10.1175/2009JAS3030.1

Cheng, A., & Xu, K.-M. (2014). An explicit representation of vertical momentum transport in a multiscale modeling framework through its 2-D cloud-resolving model component. *Journal of Geophysical Research: Atmospheres*, *119*(5), 2356–2374. https://doi.org/10.1002/2013JD021078

DeMott, C. A., Randall, D. A., & Khairoutdinov, M. (2007). Convective Precipitation Variability as a Tool for General Circulation Model Analysis. *Journal*

of Climate, *20*(1), 91–112. https://doi.org/10.1175/JCLI3991.1

DeMott, C. A., Stan, C., Randall, D. A., Kinter, J. L., & Khairoutdinov, M. (2011). The Asian Monsoon in the Superparameterized CCSM and Its Relationship to Tropical Wave Activity. *Journal of Climate*, *24*(19), 5134–5156. https://doi.org/10.1175/2011JCLI4202.1

Emanuel, K. (2021). Response of Global Tropical Cyclone Activity to Increasing CO2: Results from Downscaling CMIP6 Models. *Journal of Climate*, *34*(1), 57–70. https://doi.org/10.1175/JCLI-D-20-0367.1

Gentine, P., Pritchard, M., Rasp, S., Reinaudi, G., & Yacalis, G. (2018). Could Machine Learning Break the Convection Parameterization Deadlock? *Geophysical Research Letters*, *45*(11), 5742–5751. https://doi.org/10.1029/2018GL078202

Held, I. M., & Zhao, M. (2011). The Response of Tropical Cyclone Statistics to an Increase in CO2 with Fixed Sea Surface Temperatures. *Journal of Climate*, *24*(20), 5353–5364. https://doi.org/10.1175/JCLI-D-11-00050.1

Hersbach, H., Bell, B., Berrisford, P., Hirahara, S., Horányi, A., Muñoz-Sabater, J., et al. (2020). The ERA5 global reanalysis. *Quarterly Journal of the Royal Meteorological Society*, *146*(730), 1999–2049. https://doi.org/10.1002/qj.3803

Huang, B., Liu, C., Banzon, V., Freeman, E., Graham, G., Hankins, B., et al. (2021). Improvements of the Daily Optimum Interpolation Sea Surface Temperature (DOISST) Version 2.1. *Journal of Climate*, *34*(8), 2923–2939. https://doi.org/10.1175/JCLI-D-20-0166.1

Huang, J., & Wu, C. (2020). Effects of Microphysical Processes on the Precipitation Spectrum in a Strongly Forced Environment. *Earth and Space Science*, *7*(6), 1–9. https://doi.org/10.1029/2020EA001190

Huffman, G. J., E. F. Stocker, D. T. Bolvin, E. J. Nelkin, & Tan, J. (2019). GPM IMERG Final Precipitation L3 Half Hourly 0.1 degree x 0.1 degree V06. https://doi.org/10.5067/GPM/IMERG/3B-HH/06

Jones, T. R., Randall, D. A., & Branson, M. D. (2019a). Multiple-Instance Superparameterization: 1. Concept, and Predictability of Precipitation. *Journal of Advances in Modeling Earth Systems*, *11*(11), 3497–3520. https://doi.org/10.1029/2019MS001610

Jones, T. R., Randall, D. A., & Branson, M. D. (2019b). Multiple-Instance Superparameterization: 2. The Effects of Stochastic Convection on the Simulated Climate. *Journal of Advances in Modeling Earth Systems*, *11*(11), 3521–3544. https://doi.org/10.1029/2019MS001611

Khairoutdinov, M. F., & Randall, D. A. (2001). A cloud resolving model as a cloud parameterization in the NCAR Community Climate System Model: Preliminary results. *Geophysical Research Letters*, *28*(18), 3617–3620. https://doi.org/10.1029/2001GL013552

Khairoutdinov, M. F., & Randall, D. A. (2003). Cloud Resolving Modeling of the ARM Summer 1997 IOP: Model Formulation, Results, Uncertainties, and Sensitivities. *Journal of the Atmospheric Sciences*, *60*(4), 607–625. https://doi.org/10.1175/1520-0469(2003)060<0607:CRMOTA>2.0.CO;2

Khairoutdinov, M., Randall, D., & DeMott, C. (2005). Simulations of the Atmospheric General Circulation Using a Cloud-Resolving Model as a Superparameterization of Physical Processes. *Journal of the Atmospheric Sciences*, *62*(7), 2136–2154. https://doi.org/10.1175/JAS3453.1

Knutson, T., Camargo, S. J., Chan, J. C. L., Emanuel, K., Ho, C.-H., Kossin, J., et al. (2020). Tropical Cyclones and Climate Change Assessment: Part II: Projected Response to Anthropogenic Warming. *Bulletin of the American Meteorological Society*, *101*(3), E303–E322. https://doi.org/10.1175/BAMS-D-18-0194.1

Kuo, K.-T., Chen, W.-T., & Wu, C.-M. (2020). Effects of convection-SST interactions on the South China Sea summer monsoon onset in a multiscale modeling framework model. *Terrestrial, Atmospheric and Oceanic Sciences*, *31*(2), 211–225. https://doi.org/10.3319/TAO.2019.08.16.01

Kuo, Y.-H., Neelin, J. D., Chen, C.-C., Chen, W.-T., Donner, L. J., Gettelman, A., et al. (2020). Convective Transition Statistics over Tropical Oceans for Climate Model Diagnostics: GCM Evaluation. *Journal of the Atmospheric Sciences*, *77*(1), 379–403. https://doi.org/10.1175/JAS-D-19-0132.1

Kuo, Y.-H., Schiro, K. A., & Neelin, J. D. (2018). Convective Transition Statistics over Tropical Oceans for Climate Model Diagnostics: Observational Baseline. *Journal of the Atmospheric Sciences*, *75*(5), 1553–1570. https://doi.org/10.1175/JAS-D-17-0287.1

Liebmann, B., Hendon, H. H., & Glick, J. D. (1994). The Relationship Between Tropical Cyclones of the Western Pacific and Indian Oceans and the Madden-Julian Oscillation. *Journal of the Meteorological Society of Japan. Ser. II*, *72*(3), 401–412. https://doi.org/10.2151/jmsj1965.72.3_401

Ma, H.-Y., Xie, S., Boyle, J. S., Klein, S. A., & Zhang, Y. (2013). Metrics and Diagnostics for Precipitation-Related Processes in Climate Model Short-Range Hindcasts. *Journal of Climate*, *26*(5), 1516–1534. https://doi.org/10.1175/JCLI-D-12-00235.1

Ma, H.-Y., Zhou, C., Zhang, Y., Klein, S. A., Zelinka, M. D., Zheng, X., et al. (2021). A multi-year short-range hindcast experiment with CESM1 for evaluating climate model moist processes from diurnal to interannual timescales. *Geoscientific Model Development*, *14*(1), 73–90. https://doi.org/10.5194/gmd-14-73-2021

Mooers, G., Pritchard, M., Beucler, T., Ott, J., Yacalis, G., Baldi, P., & Gentine, P. (2021). Assessing the Potential of Deep Learning for Emulating

Cloud Superparameterization in Climate Models With Real-Geography Boundary Conditions. *Journal of Advances in Modeling Earth Systems*, *13*(5), 1–26. https://doi.org/10.1029/2020MS002385

Moseley, C., Henneberg, O., & Haerter, J. O. (2019). A Statistical Model for Isolated Convective Precipitation Events. *Journal of Advances in Modeling Earth Systems*, *11*(1), 360–375. https://doi.org/10.1029/2018MS001383

Oouchi, K., Yoshimura, J., Yoshimura, H., Mizuta, R., Kusunoki, S., & Noda, A. (2006). Tropical Cyclone Climatology in a Global-Warming Climate as Simulated in a 20 km-Mesh Global Atmospheric Model: Frequency and Wind Intensity Analyses. *Journal of the Meteorological Society of Japan. Ser. II*, *84*(2), 259–276. https://doi.org/10.2151/jmsj.84.259

Patricola, C. M., & Wehner, M. F. (2018). Anthropogenic influences on major tropical cyclone events. *Nature*, *563*(7731), 339–346. https://doi.org/10.1038/s41586-018-0673-2

Pritchard, M. S., Bretherton, C. S., & DeMott, C. A. (2014). Restricting 32-128 km horizontal scales hardly affects the MJO in the Superparameterized Community Atmosphere Model v.3.0 but the number of cloud-resolving grid columns constrains vertical mixing. *Journal of Advances in Modeling Earth Systems*, *6*(3), 723–739. https://doi.org/10.1002/2014MS000340

Pritchard, M. S., & Somerville, R. C. J. (2009). Assessing the diurnal cycle of precipitation in a multi-scale climate model. *Journal of Advances in Modeling Earth Systems*, *2*(4), 12. https://doi.org/10.3894/JAMES.2009.1.12

Randall, D., DeMott, C., Stan, C., Khairoutdinov, M., Benedict, J., McCrary, R., et al. (2016). Simulations of the Tropical General Circulation with a Multiscale Global Model. *Meteorological Monographs*, *56*, 15.1-15.15. https://doi.org/10.1175/AMSMONOGRAPHS-D-15-0016.1

Rasp, S., Pritchard, M. S., & Gentine, P. (2018). Deep learning to represent subgrid processes in climate models. *Proceedings of the National Academy of Sciences*, *115*(39), 9684–9689. https://doi.org/10.1073/pnas.1810286115

Roberts, M. J., Camp, J., Seddon, J., Vidale, P. L., Hodges, K., Vannière, B., et al. (2020). Projected Future Changes in Tropical Cyclones Using the CMIP6 HighResMIP Multimodel Ensemble. *Geophysical Research Letters*, *47*(14), 1–12. https://doi.org/10.1029/2020GL088662

Tao, W.-K., & Chern, J.-D. (2017). The impact of simulated mesoscale convective systems on global precipitation: A multiscale modeling study. *Journal of Advances in Modeling Earth Systems*, *9*(2), 790–809. https://doi.org/10.1002/2016MS000836

Villafuerte, M. Q., Lambrento, J. C. R., Hodges, K. I., Cruz, F. T., Cinco, T. A., & Narisma, G. T. (2021). Sensitivity of tropical cyclones to convective parameterization schemes in RegCM4. *Climate Dynamics*, *56*(5–6), 1625–1642. https://doi.org/10.1007/s00382-020-05553-3

Wu, L., Liang, J., & Wu, C.-C. (2011). Monsoonal Influence on Typhoon Morakot (2009). Part I: Observational Analysis. *Journal of the Atmospheric Sciences*, *68*(10), 2208–2221. https://doi.org/10.1175/2011JAS3730.1

Zarzycki, C. M. (2022). Sowing Storms: How Model Timestep Can Control Tropical Cyclone Frequency in a GCM. *Journal of Advances in Modeling Earth Systems*, *14*(3), 1–21. https://doi.org/10.1029/2021MS002791

Zhang, Y., Klein, S. A., Liu, C., Tian, B., Marchand, R. T., Haynes, J. M., et al. (2008). On the diurnal cycle of deep convection, high-level cloud, and upper troposphere water vapor in the Multiscale Modeling Framework. *Journal of Geophysical Research*, *113*(D16), D16105. https://doi.org/10.1029/2008JD009905

Zhao, M., Held, I. M., & Lin, S.-J. (2012). Some Counterintuitive Dependencies of Tropical Cyclone Frequency on Parameters in a GCM. *Journal of the Atmospheric Sciences*, *69*(7), 2272–2283. https://doi.org/10.1175/JAS-D-11-0238.1